SunBox: Screen-to-Camera Communication with Ambient Light

MIGUEL CHÁVEZ TAPIA*, Delft University of Technology, The Netherlands

TALIA XU, Delft University of Technology, The Netherlands

ZEHANG WU, Delft University of Technology, The Netherlands

MARCO ZÚÑIGA ZAMALLOA, Delft University of Technology, The Netherlands

A recent development in wireless communication is the use of optical shutters and smartphone cameras to create optical links solely from *ambient light*. At the transmitter, a liquid crystal display (LCD) modulates ambient light by changing its level of transparency. At the receiver, a smartphone camera decodes the optical pattern. This LCD-to-camera link requires low-power levels at the transmitter, and it is easy to deploy because it does not require modifying the existing lighting infrastructure. The system, however, provides a low data rate, of just a few tens of bps. This occurs because the LCDs used in the state-of-the-art are slow *single-pixel* transmitters. To overcome this limitation, we introduce a novel *multi-pixel* display. Our display is similar to a simple screen, but instead of using embedded LEDs to radiate information, it uses *only* the surrounding ambient light. We build a prototype, called SunBox, and evaluate it indoors and outdoors with both, artificial and natural ambient light. Our results show that SunBox can achieve a throughput between 2 kbps and 10 kbps using a low-end smartphone camera with just 30 FPS. To the best of our knowledge, this is the first screen-to-camera system that works solely with ambient light.

CCS Concepts: • **Computer systems organization** → **Embedded systems**; • **Human-centered computing**;

Additional Key Words and Phrases: visible light communication, backscattering, ferroelectric liquid crystal over silicon, screen-camera communication

1 INTRODUCTION

Due to the ever-increasing demand for bandwidth in the radio-frequency spectrum, there has been a growing interest in exploiting other portions of the electromagnetic spectrum, in particular, with a novel technology called visible light communication (VLC). In no small part, this interest is due to the pervasive presence of various types of LEDs in our environments (acting as transmitters) and cameras on mobile devices (acting as receivers).

Broadly speaking, there are two kinds of optical links using light sources as transmitters and smartphones as receivers: LED-to-camera and screen-to-camera. In these two systems, the light sources transmit information by modulating their intensity at relatively high speeds (hundreds of Hz), and smartphones capture these patterns with cameras that usually operate between 30 to 120 frames-per-second (FPS). When a single LED is used for transmission, every captured frame contains one bit or at most a few bits of information. LED-to-camera links

---

*Corresponding author

Authors' addresses: Miguel Chávez Tapia, m.a.chaveztapia@tudelft.nl, Delft University of Technology, Delft, The Netherlands; Talia Xu, Delft University of Technology, Delft, The Netherlands, m.xu-2@tudelft.nl; Zehang Wu, Delft University of Technology, Delft, The Netherlands, z.wu-7@student.tudelft.nl; Marco Zúñiga Zamalloa, Delft University of Technology, Delft, The Netherlands, m.a.zunigazamalloa@tudelft.nl.

are simple to implement but result in low data rates. Depending on the type of modulation, binary or rolling shutter, those systems achieve from less than 100 bps [2, 33] to 100 kbps [6, 18, 34]. Screens, on the other hand, contain millions of tiny LEDs (pixels). With those pixels, displays can create more complex patterns, similar to QR codes, containing thousands of bits on every frame. This property enables screen-to-camera links to reach data rates beyond 100 kbps [8, 23, 27, 36, 37].

The above systems are enabling a wide range of new applications, from indoor positioning [16, 30] and human-computer-interaction [2, 33], to streaming services [25, 37]. The *transmitters* of these systems, however, have two limitations. First, they require modifying the operation of the light source (LED or screen), which is not always possible. Second, they often require a significant amount of power. For example, a standard LED bulb can consume several watts, and a simple monitor requires several tens of watts.

To overcome the above limitations, researchers are proposing *passive* methods that use *ambient light* for communication. Contrary to the aforementioned *active* systems, which require direct control of the light source to modulate its intensity, *passive* methods work with any ambient light, natural (coming from the sun) or artificial (coming from a light bulb). The basic principle of most *passive* systems is to modulate the intensity of ambient light using liquid crystals. A liquid crystal (LC) cell placed between two polarizers can be seen as an optical shutter that switches between opaque and semi-transparent states to transmit logical 0s and 1s. In these novel *LCD-to-camera* systems, the LCD transmitters consume power in the order of a few tens of mW and do not require any modification of the light source [35].

Challenge. Similar to LED-to-camera systems, the main limitation of current LC-to-camera links is their low data rate. The problem of using a single LED (or a single LC cell) is that the transmitter only has a single pixel to send information. To increase the data rate, we require a multi-pixel modulating surface, similar to a screen but operating with the surrounding ambient light.

Contributions. Motivated by advances in reflective display technology, which backscatters sunlight to create images [24], we propose the first screen-to-camera system that works solely with ambient light. The aim is to deploy small screens, a few millimeters in size, so users can place their phone near the screen to receive data: *such a system implements an optical wireless link with a range similar to near-field communication (NFC) technology but using ambient light as the carrier and the smartphone's camera as a receiver.* Our system, called *SunBox*, will enable all types of smartphones, from low- to high-end, to rely only on their camera to obtain a near-field optical link. Overall, our work provides three main contributions.

Contribution 1 [section 3]: A system that achieves secure screen-to-camera communication with ambient light. Taking as a basis a tiny projector designed for near-eye applications (short-range projection), we propose a novel optical design that removes the embedded LEDs of the original system so it can operate solely with ambient light. The system is enclosed in a custom-designed 3D box that prevents eavesdropping.

Contribution 2 [section 4]: A robust optical link under varying lighting conditions. SunBox is designed to work indoors, with different types of artificial lighting; and outdoors, where the spectrum and intensity of sunlight change constantly. This wide range of conditions affects the performance of the optical link. We combine various signal processing and error-correcting methods to provide reliable ambient light communication.

Contribution 3 [section 5 and section 6]: A prototype implementation and a thorough evaluation. We build a prototype and test it with different types of phones, data densities and ambient light. Considering all these variables, our results show that the goodput reaches between 2 and 10 kpbs, providing reliable connections indoors and outdoors, even with low-end phones.

Table 1. Wireless short-distance communications

Protocol	Throughput	Power	Band	Presence in phones	Interference in the same band
BLE	2 Mpbs	~50 mW	Radio	~100%	WiFi, Zigbee, microwave oven
NFC	424 kbps	~30 mW	Radio	~60%	RFID
Pulse[13]	44 bps	~0.83 mW	Magnetic Field	~100%	Appliances with high magnetic induction
MagneComm[22]	110 bps	~5.2 W	Magnetic field	~100%	Appliances with high magnetic induction
Sunbox	(2–10) kbps	~110 mW	Visible Light	~100%	-

2 BACKGROUND

2.1 Short-Distance Wireless Technology

Traditional short-distance wireless links, like NFC or Bluetooth Low Energy (BLE) use radio waves as their carrier and their hardware modules consume low power. BLE is widely adopted and NFC hardware is available in around 60% of smartphones[1]. However, both are prone to interference with other signals in the radio-frequency spectrum.

To overcome this limitation, the research community has proposed the use of magnetic fields, such as Pulse[13] and MagneComm[22]. These approaches exploit the magnetic sensor present in all smartphones, but it has a limited data rate and it is exposed to the magnetic field created by different appliances. Our work presents SunBox. An approach that uses the free and open spectrum provided by ambient light and requires only a camera as a receiver, which is present in virtually all smartphones. SunBox achieves data rates that are orders of magnitude higher than magnetic approaches while consuming less power than some of them. Table 1 positions the pros and cons of SunBox with respect to other short-distance wireless technologies. In the next sections, we analyze different types of displays to find the best fit for our screen-to-camera approach.

2.2 Identifying the Right Type of Display

Display technology offers different options for various kinds of scenarios. A popular option is e-ink, but it is too slow, as it offers refresh rates of ~3 Hz. Among other low-power display technologies, two types have (partial) properties suitable for SunBox: microdisplays and reflective displays.

Microdisplays are small, a few mm in size, and they are designed to work in enclosed near-eye applications, such as virtual reality headsets. This setup is similar to the one envisioned for SunBox, where the enclosed environment provides a secure optical link because the image is projected only to the intended receiver. The main limitation is that microdisplays require embedded LED lights to operate. *Reflective displays*, on the other hand, do not need embedded artificial lights, they simply reflect ambient light to render an image. Reflective displays are particularly suitable for outdoor deployments because they achieve a high contrast under sunlight. The shortcomings of reflective displays are their *size*, there are no micro-display versions, and their inherent *broadcast nature*, the field of view is broad. These two shortcomings would allow eavesdropping.

Our application, secure short-range communication using ambient light, requires a microdisplay but with reflective properties. Next, we describe various microdisplay technologies and identify one that will allow us to remove the embedded LEDs and re-design the optical enclosure to work as a reflective display with ambient light.

2.3 Microdisplays for Short-range Communication

Microdisplay technologies include micro-OLED, Digital Micro-mirror Devices (DMDs) and Liquid Crystal over Silicon (LCoS). We are looking for two properties in their optical designs, the possibility to disconnect the LEDs

---

[1]NFC Forum: https://nfc-forum.org/fresh-smartphone-statistics-and-what-they-mean-for-you-nfc-and-the-world/

(a) Single cell with two polarizers.   (b) Reflective display (array of LC cells).   (c) *Nematic*: $t_{ON} \neq t_{OFF}$.   (d) *Smectic*: $t_{ON} = t_{OFF}$
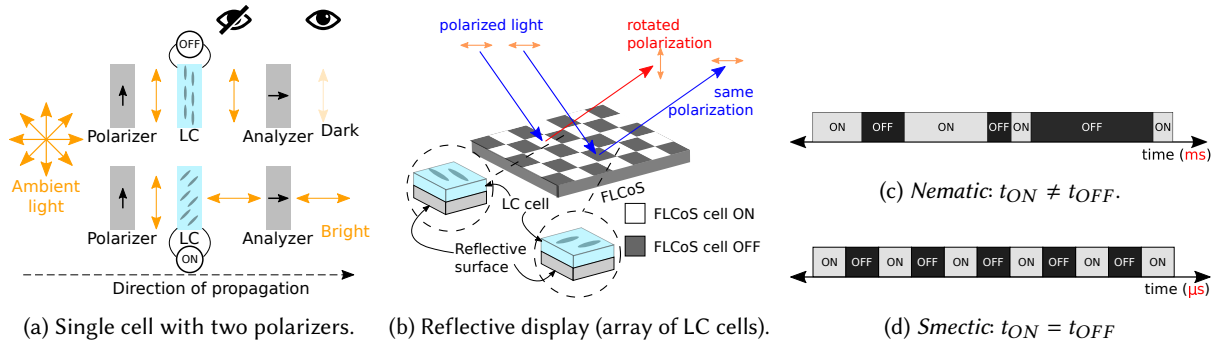
Fig. 1. (a, b) Basic LC modulation and (c,d) the operational difference of LCs. ON and OFF are polarization states set by the control voltage.

and the ability to backscatter light. Micro OLED displays have tightly integrated organic LEDs. DMD and LCoS displays, on the other hand, work as reflective surfaces with hundreds of thousands of pixels. Embedded LEDs radiate light onto the pixels, which either reflect or absorb light to render the image.

DMD and LCoS are, in principle, suitable for our application. Their embedded lights can be removed, they use backscattering surfaces, and they have similar low-power consumption. Their main difference is the reflective material. DMDs use an array of micro-mirrors that are moved mechanically between two fixed angles: towards the intended receiver or towards a light absorber. These micro-mirrors work well with custom-designed LEDs that provide constant illumination at the same incidence angle, but sunlight is variable and changes its direction throughout the day. LCoS do not have strong constraints for the incoming light. Instead of mechanical movements, they use liquid crystals above a layer of reflective coating with a wide incident angle. This property makes them suitable to operate with various types of light.

The more relaxed requirement for the incident angle is a key factor for our system to work indoors and outdoors. Next, we describe in more detail the operation of LCoS, and the difference with other types of LCs used in the SoA. This background is necessary to understand the optical modifications required to make LCoS work with ambient light, as will be discussed in section 3.

2.4 Types of LCoS Microdisplays

LCs have the ability to change the polarization of light and are commonly used as optical shutters, as shown in Figure 1a. First, a light source emits unpolarized light, which passes through a first polarizer. Then, depending on the applied voltage on the LC, the polarization direction remains the same or rotates 90°. A second polarizer, called *analyzer*, either blocks or allows the passing of light. Microdisplays have hundreds of thousands of tiny LC cells, each a few microns in size, and every cell (pixel) exploits the above principle. The important difference of LCoS is the presence of the reflective layer under the LC cell, as shown in Figure 1b. LCoS has the potential to work with external sources (like sunlight) because the light rays are reflected off the surface[2].

A central property of an LC cell is the switching speed between its two states. The faster the speed, the more colors a display can convey[3]. The pixels are manufactured with different types of LCs, called *mesophases*, and the two main are *nematic* and *smectic*, depicted in Figure 1c and Figure 1d, respectively.

---

[2]Note that sunlight, like artificial light, is unpolarized. Thus, reflective displays still need the polarizers shown in Figure 1a to operate.

[3]Displays create colors by duty-cycling their pixels. For example, an image transmitted at 60 Hz is decomposed into its RGB components (180 Hz). Denoting the period of each primary color as $T = \frac{1}{180\,Hz}$, the colors red and white are conveyed by keeping a pixel ON for T and 3T, respectively. But a shade of red, say at 10%, requires a pixel to be ON only for 0.1T. Hence, faster pixels can render more color combinations.
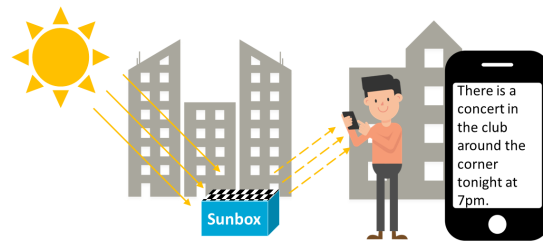
Fig. 2. Overview of SunBox. A microdisplay reflects encoded ambient light to a smartphone camera placed at close range.

Nematic LCs have slow and asymmetric response times but allow a flexible control. The rise and fall times are in the order of ms and the fall time is slower than the rise time. On the positive side, any status of the cell (on or off) can be maintained for an arbitrary period, which allows flexibility in the modulation process.

Smectic LCs have symmetric and fast response times, in the order of tens of μs, which allow refresh rates as high as 360 Hz. On the negative side, they have a relatively rigid operation. Due to their internal molecular alignment, the modulation has to switch constantly between the two polarization states and needs to maintain, on average, a 50 % duty cycle.

Current research in ambient light communication focuses on *big nematic* LCs [3, 17, 29, 31, 32, 35]. Those LCs lead to designs that are simple and low-cost, but *bulky* (the area of a single cell is bigger than 10 cm^2) and *slow* (the data rate of *single-pixel transmitters* using cameras as receivers is below 100 bps, and around 1 kbps when photodiodes are used as receivers). We use a microdisplay based on Ferroelectric LCoS (FLCoS), a type of smectic LC, that is designed to work with tightly synchronized LEDs. In section 3, we show that, after removing the embedded LEDs, the duty-cycling requirement of smectic LCs poses non-trivial challenges to make them work with ambient light.

2.5 Data Representation

Having a screen at the transmitter enables the modulation of 2D codes. The design of these codes needs to balance range, reliability, and throughput. SunBox aims at short-distance communication in the range of centimeters, hence our main trade-off is between reliability and throughput. Prior studies using traditional screens as transmitters have either used well-known standards [19], such as QR codes, or defined their own customary code [15, 37]. We use standard codes because they are designed to have high-density capabilities, error correction, and resilience to image distortion.

Two standards are widely used for 2D codes: QR and Datamatrix. The pixels in 2D codes are divided into two main areas: recognition (masks, alignment, etc.) and data (information plus error correction). A Datamatrix can carry more information because fewer pixels are used for *recognition*[4], but we select QR codes for two main reasons. First, Datamatrices have a fixed 30% error correction overhead, while QR codes are more flexible, allowing 7%, 15%, 25%, and 30%. Second, QR technology is more mature and widely deployed in mobile applications, which eases the code generation and decoding processes. In our evaluation, however, we also present results with Datamatrices to showcase the generality of our approach to different formats and data densities.

3 PASSIVE MICRODISPLAY-TO-CAMERA COMMUNICATION

We propose a passive communication system, depicted in Figure 2, that has three main components: an emitter (any type of light source, natural or artificial), a transmitter (a screen that backscatters 2D patterns with ambient

---

[4]Approximately, a Datamatrix uses 15% of the area for recognition, while QR codes use 25%.
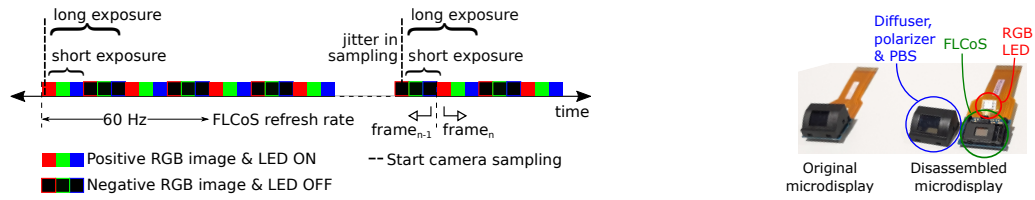
(a) Time sequence of the FLCoS RGB-color sub-framing and the camera exposure time.

(b) Disassembly of microdisplay.

Fig. 3. Operation and components of the microdisplay. In(b), the black cap contains a polarizer and a diffuser for the RGB LED, and a polarizing beam splitter (PBS), which works as the analyzer. Removing this cap gives access to the FLCoS

light), and a receiver (a smartphone camera). To provide a user interface, a keyboard could be added to allow the user to enter a specific code. In this section, we focus on the design of the transmitter. First, we describe the original off-the-shelf microdisplay, which contains various optical and lighting components in addition to the microdisplay itself, and then, we present our design which removes all these components and proposes a novel design that works solely with ambient light.

3.1 Off-the-Shelf Microdisplay

We build our system based on the LCOS720 micro-projector from Control Electronic [20]. It has a small microdisplay with a diagonal size of 5 mm and is used for short-range near-eye applications, such as augmented reality headsets. The microdisplay is based on FLCoS technology and has a resolution of 720x540 pixels, a video refresh rate of 60 Hz, and costs 70€.

The LCOS720 micro-projector works in the following manner. Inside the projector, embedded RGB lights are integrated with polarizer screens. Polarized rays reach the microdisplay and are reflected with either the same polarization (pixel on) or with a rotated polarization that is blocked by the analyzer (pixel off), similar to the design in Figure 1b. In principle, the ability to backscatter the incident light allows the microdisplay to be used with any ambient light, instead of dedicated RGB lights.

However, in spite of the backscattering property, transforming the FLCoS display into an ambient light display is not as trivial as simply removing the 'unnecessary' components of the original micro-projector (LED lights, Polarized Beam Splitters, etc.). The intrinsic 50% duty cycle of the smectic LCs requires a fundamentally different system design to work with ambient light.

3.2 Benchmark with Original Display

The FLCoS display renders color by dividing each frame into six sub-frames for red, green, and blue: *RGBRGB*. To satisfy the duty cycle requirement of smectic LCs, every time a pixel is *on* for a given color, it has to be *off* for the same period. Hence, the frames also need to include the negative states: $RGB\overline{RGB}RGB\overline{RGB}$. To project the intended image, the device tightly synchronizes its RGB LED to illuminate *only* the *positive* pulses (*RGB*), as shown in Figure 3a. To capture the radiated image, cameras average the light intensity received over the *exposure time*, as illustrated in Figure 3a. Depending on the exposure time, a camera may capture only part of the *RGB* pulses (resulting in a colored code) or a full RGB period (resulting in a black&white code), as shown in Figure 4b. The exposure time can be set initially via the exposure value (EV) parameter, but it changes in time according to the amount of ambient light. In general, the darker the environment, the longer the exposure time.

3.2.1 Setup. The setup we use to test the micro-display is depicted in Figure 4a. The display transmits QR codes at 15 FPS, and it is positioned 10 cm away from a Xiaomi Redmi 5A (a low-end phone), which captures the frames at 30 FPS. To recreate an enclosed casing, we carry out the experiments in a dark environment.
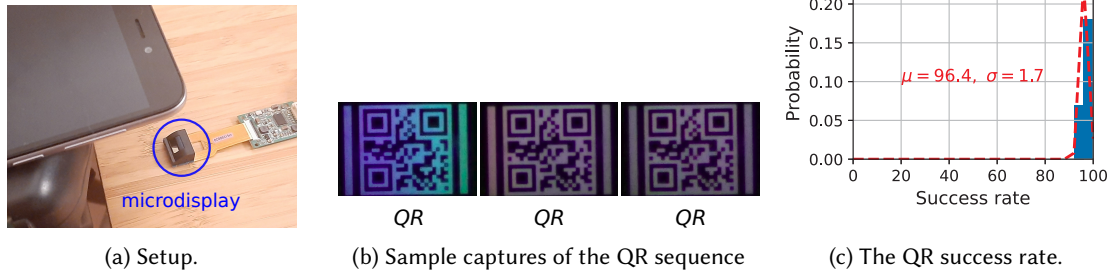
(a) Setup.

(b) Sample captures of the QR sequence

(c) The QR success rate.

Fig. 4. Results using COTS microdisplay

(a) Photodiode (PD) setup.
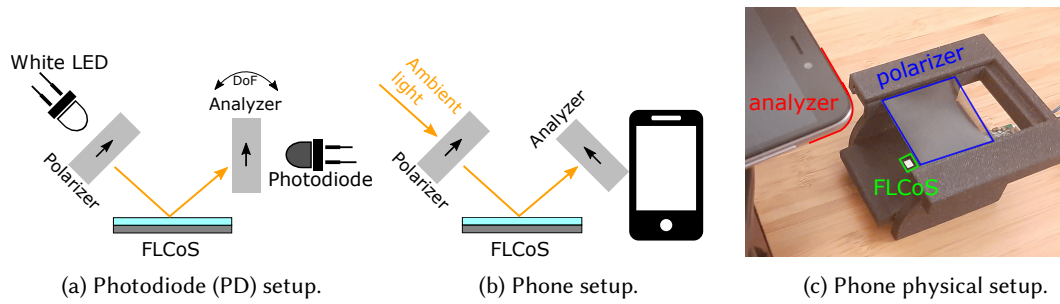
(b) Phone setup.

(c) Phone physical setup.

Fig. 5. Setups for experiments using the FLCoS. For each setup, the second polarizer (analyzer) has a degree of freedom (DoF) to change its orientation w.r.t the first polarizer.

3.2.2 Processing. SunBox requires tailored signal processing and error correction methods to work reliably (section 4). However, to set a baseline for our evaluation, we use a basic processing toolchain. An *OpenCV* script is used to identify the area of the FLCoS screen, and the *ZXing* library is used to decode the QR codes.

3.2.3 Results. We transmit 100 messages, each containing 100 QR codes. Figure 4c shows the statistical distribution of the *success rate*, which is defined as the percentage of QR codes decoded in a message. As expected, most QR codes are decoded, with a success rate of 96.4 %±1.7 %. Occasionally the camera misses a frame, which can be caused due to jitter or because the exposure time is long and gets close to the frame rate of the transmitter [1, 5].

We will see next that the high success rate of the original projector gets severely affected when the embedded lights are removed and the system operates with ambient light.

3.3 FLCoS with Ambient Light

The operation with ambient light is different from the operation with the embedded RGB LED in two key aspects: a lack of synchronization with the positive pulses and a shorter exposure time due to a more illuminated environment. Both effects, combined with the inherent jitter of the camera, mean that the exposure time can cover positive pulses (RGB), negative pulses ($\overline{RGB}$), or their combination, rendering a low contrast QR, its negative version, or gray images, respectively. To highlight these effects, we assess the modified system with ambient light.

3.3.1 Setup. After removing the embedded RGB LED (Figure 3b), we consider two setups. The first setup is used to capture the reflection properties of all pulses: $RGB\overline{RGB}$. This setup uses an external flashlight as the light source and a photodiode as a receiver (Figure 5a), which has a higher sampling rate and allows capturing in

(a) COTS FLCoS with cross polarizers.

(b) FLCoS with cross polarizers and no alignment layer.

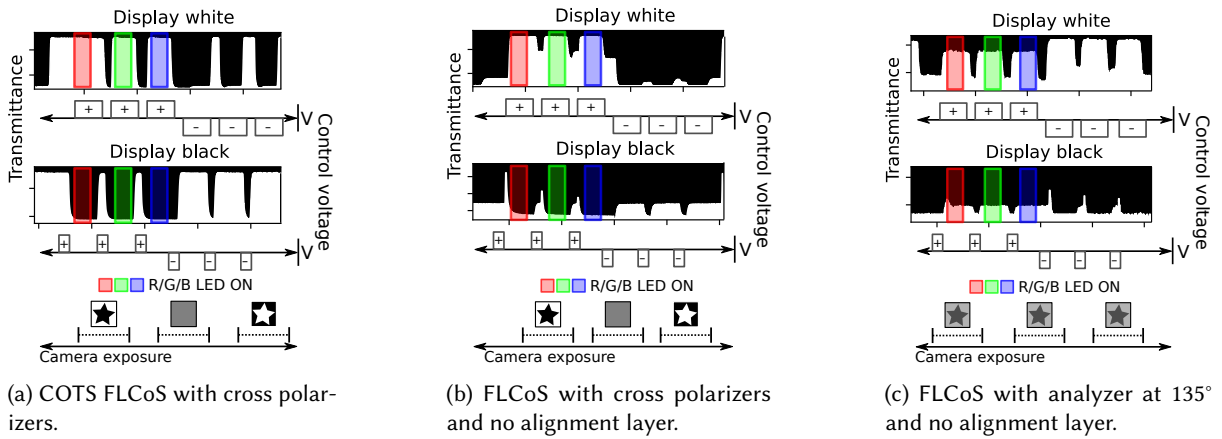(c) FLCoS with analyzer at 135° and no alignment layer.

Fig. 6. Output of the photodiode for the setup in Figure 5a. Each plot shows the sequence of voltage pulses. And, at the bottom of each figure, we show the expected images (positive, negative or gray) for different exposure times.

detail the pulses' trend. The second setup is used to capture the success rate (Figure 5b). This setup uses the phone as a receiver and considers only the ambient light present in the room, around 500 lx, which is the average illuminance in an office space. Since the FLCoS requires two polarizers to work, c.f. Figure 1, a polarizer is placed on top of the FLCoS and an analyzer in front of the photodiode or camera.

3.3.2 Results. For the first setup (flashlight & photodiode), we send a series of white and black screens. Figure 6a shows the results. The top plot depicts the pulses for the white screen and the bottom for the black screen. In both cases, we can see the $RGB\overline{RGB}$ trend. Note that both screen colors need to maintain an average duty cycle of 50%. Below the plots, we place sample exposure times to showcase the possibility of getting positive, negative, or gray images. For the second setup (ambient light & camera), we send 100 messages with 100 QR codes each. A few samples of the captured frames are displayed in Figure 7a, showing (as expected):

- *Positive (normal) image:* when the exposure time covers only (mainly) the regular pulses RGB. Note that even in this "optimal" case, the contrast is lower than the one obtained with embedded LEDs (c.f. Figure 4).
- *Negative image:* when the exposure time covers only (mainly) the negative pulses $\overline{RGB}$. In this case, the color of the image is inverted.
- *Gray image:* when the exposure time covers partially the regular and negative pulses, the intensity of the colors averages out, rendering an unreadable gray screen.

The negative and gray images, which the system cannot decode, cause the success rate to drop drastically to 31.9 %±3.8 %, as illustrated in Figure 7d. Next, we propose two methods to eliminate these types of images.

3.4 FLCoS without the *Alignment Layer*

A unique (and counter-intuitive) feature of smectic LCs is that rendering both, black and white screens, require providing and blocking illumination, c.f. Figure 6a. This behavior is widely different from the nematic LCs used in the SOA [3, 17, 29, 31, 32, 35, 37]: the white state, set by V_+, provides illumination, and the black state, set by V_0 (ground voltage), blocks it. Smectic LCs, on the other hand, need to balance the polarization states by using three voltages: V_+, V_-, and V_0, and an *alignment layer*. Due to the effect of the *alignment layer*, the transitions from V_+ to V_0 block illumination and from V_- to V_0 provide it. With these transitions, the positive pulses (RGB)
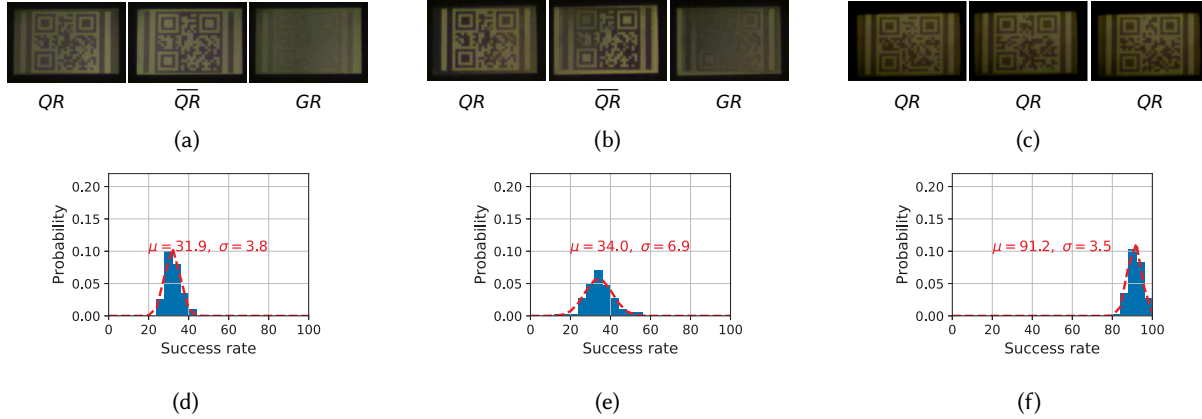
Fig. 7. Output of the camera for the setup in Figure 5b. FLCoS and cross polarizers: (a) & (d). FLCoS with cross polarizers and no alignment layer: (b) & (e). FLCoS with analyzer at 135° and no alignment layer: (c) & (f). The left column shows sample QR codes and the right column the QR success rate.

require sending a series of (V_+, V_o), and the negative pulses ($\overline{RGB}$) require sending a series of (V_-, V_o), as depicted in the voltage plots of Figure 6a.

The *alignment layer* simplifies the control signals required by the smectic LC because switching between the orthogonal states requires only removing the driving voltages. For our purposes, this continuous switching makes it highly probable for a camera to capture low-contrast or gray images. Motivated by research studies that analyze the properties of smectic FLCs [7, 10, 14], we hypothesize that by releasing the FLCoS from the alignment layer, we could get illumination patterns that will increase the contrast between the black and white states across time.

3.4.1 Setup. Since the microdisplay is contained in one package, we release the alignment layer from the FLCoS by mechanically releasing the pressure of the package[5]. Afterward, we test the same setups of our prior experiment: flashlight & photodiode to capture the reflected patterns, and ambient light & camera to capture the success rate.

3.4.2 Results. Figure 6b shows the results for the reflected patterns. Without the alignment layer, the white display has a clearer alternating pattern between high and low, and the black display is mainly low. This setup still renders gray and negative images (Figure 7b). Thus, the success rate improves minimally to 34.0 %±6.9 %. In the next section, we show that a particular type of *phase modulation* provides a final solution to creating a screen-to-camera link with ambient light.

3.5 Phase Modulation: Removing *Negative and Gray Images*

The main limitation of the previous steps is the presence of gray and negative images. Adding *phase modulation* [21] will remove these issues. In essence, the alignment layer forces the FLCoS to have only two possible polarization states: parallel or orthogonal to the analyzer (Figure 8a). Thus, all pixels –black and white– are limited to using a combination of bright and dark polarizations to render their desired state. The removal of the alignment layer *releases* a wider range of polarization states (Figure 8b) because they are no longer forced to be in either of the two states. For a white pixel, the polarization state presents two clusters, one cluster is close to the parallel orientation

---

[5]The process was repeatedly applied to several FLCoS with similar results.

(a) Original FLCoS.   (b) FLCoS without alignment layer.   (c) FLCoS with analyzer at 135°
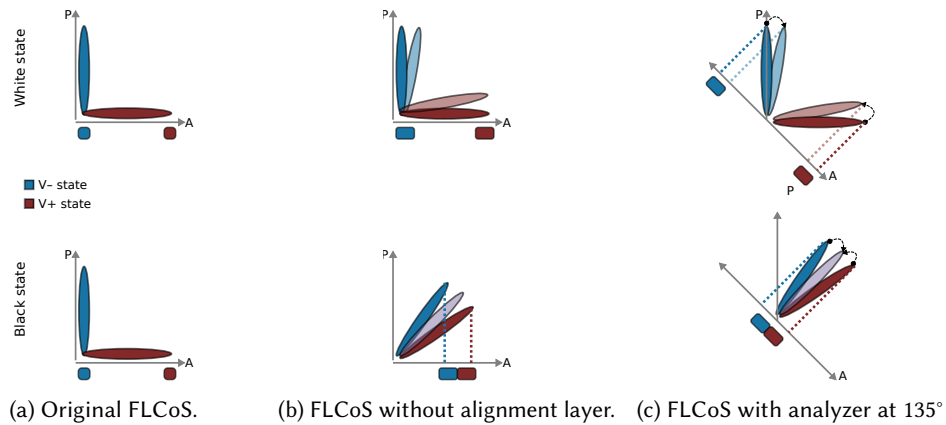
Fig. 8. Transformation of the polarization domain. The P-axis reflects the angle of the polarizer, and the A-axis the angle of the analyzer. (a) With the alignment layer, the black and white displays only project two intensity levels: bright and dark. (b) Without the alignment layer, the white display remains relatively close to the original polarization states, but the black display shifts its brightness towards a cluster centered around 45°. (c) Phase modulation creates new projections, the black display becomes relatively dark, while the two clusters of the white display render medium-brightness.

of the analyzer (bright) and the other cluster is close to the orthogonal orientation (dark). For a black pixel, there is a single cluster, approximately at 45° from the analyzer (medium brightness). If we rotate the analyzer to an angle of 135° (Figure 8c), the black cluster becomes orthogonal to the analyzer, rendering a darker tone, and the two white clusters get projected to *similar* magnitude values, rendering brighter tones.

Note that this phase modulation method would not work if we do not release the alignment layer. With a 135° analyzer, the white and black states in Figure 8a would project to the same medium-brightness levels, making them indistinguishable from each other.

3.5.1 Setup. To evaluate our joint solution, releasement of the alignment layer, and phase modulation, we test the same setups with the photodiode and camera, but with the analyzer at an angle of 135° w.r.t. the polarizer.

3.5.2 Results. Figure 6c shows the reflection of the pulses, and we can notice that, in spite of the 50% duty cycle, we are able to provide different intensities for the white and black states across the entire time. For a white screen, the illuminance provides a medium-to-high brightness, and for a black screen, the illuminance switches between two low-brightness states. Figure 7c shows that changing the angle eliminates the *negative* and *gray images*, which boosts the QR success rate to 91.2 %±3.5 %, as illustrated in Figure 7f.

3.6 Trade-off of Eliminating *Negative and Gray Images*

The main side-effect of the transformation of the polarization domain is the reduction of contrast between bright and dark states. Table 2 shows the contrast for all the setups in this section. Despite the low contrast of the SunBox setup, the QR success rate improves to 91.2 %, similar to the original microdisplay. In the next section, we present some techniques to deal with low-contrast images and variable light intensities.

4 ATTAINING RELIABLE LINKS

The prior section describes the optical design required to use FLCoS with ambient light. The images, however, can still appear distorted due to the variable and noisy nature of ambient light. In this section, we present the methods used to overcome those limitations in order to provide reliable links.

(b) Equalization.

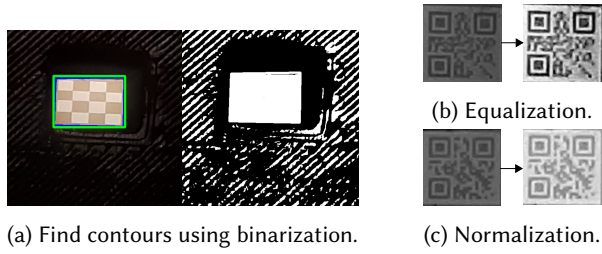(c) Normalization.

(a) Find contours using binarization.

Fig. 9. Frame processing. Figure (a) shows a sample frame [left] and its binarized version [right]. The ROI is captured by a green contour. Figures (b) and (c) are the signal processing methods used to enhance the images within the ROI.

Table 2. Image contrast for different setups.

Feature	RGB LED	Ambient Light	
		Cross-polarizers	SunBox
Contrast	$40 \pm 5\,\%$	$17 \pm 3\,\%$	$11 \pm 1\,\%$
White*	170 ± 27	163 ± 9	156 ± 6
Black*	0	27 ± 16	49 ± 5

* Intensity values range between 0 and 255.

Unless stated otherwise, the following libraries are used in the development of the smartphone App: *OpenCV* for signal processing, *ZXing* for QR decoding, and *Backblaze's JavaReedSolomon*[6] for error correction.

4.1 Detecting the Region-of-Interest (ROI)

In the experiments done so far, the detection of the region of interest was a manual process. To ease this requirement, we implement an automatic detection process. The detection takes advantage of the reflective nature of the FLCoS, which is surrounded by a dark and opaque surface. Therefore, the camera sees the FLCoS as a high-brightness area over a dark background and performs the following three steps to detect the ROI:

- *Binarization:* the adaptiveThreshold function renders a black and white image (Figure 9a).
- *Rectangle detection*: the findContours function detects all shapes, and the approxPolyDP function approximates the shapes to the closest polygon.
- *Rectangle selection:* we filter rectangles by ratio and size. The aspect ratio of the FLCoS is 4:3, and we filter out rectangles larger than 2% and smaller than 20% of the entire screen.

The identified region is then sent to the QR library. The ROI method reduces the computation time and increases the QR success rate. Handling the entire frame takes ∼205 ms and has a 65 % success rate, whereas handling only the ROI takes ∼140 ms and has a 100 % success rate. This ROI method is used in the remainder of the paper.

4.2 Enhancing the Image Quality for Dawn and Dusk

Thus far, the system has been tested under constant and direct ambient light (∼500 lx). However, we need to consider diffuse conditions with low light, such as those present during dusk and dawn or in low-lit indoor scenarios. We implement a simple toolchain to increase the contrast under those conditions. The tool chain uses equalization (equalizeHist) and normalization (normalization), as depicted in Figure 9b and Figure 9c.

These signal processing methods have a minor effect under normal ambient light conditions. For example, with the setup used in section 3, the success rate increments scarcely from 91.2 % to 92.5 %, but the contribution of the methods is more noticeable in challenging setups. To assess this effect, we attenuate the light reaching the FLCoS. Using this low-lit setup, the signal processing stage increases the success rate from 70 % to 85 %.

4.3 Creating a Reliable Simplex Link

SunBox implements a simplex channel with no feedback nor re-transmission of lost frames. Thus, to obtain a reliable link, SunBox requires the use of Forward-Error-Correction methods (FEC).

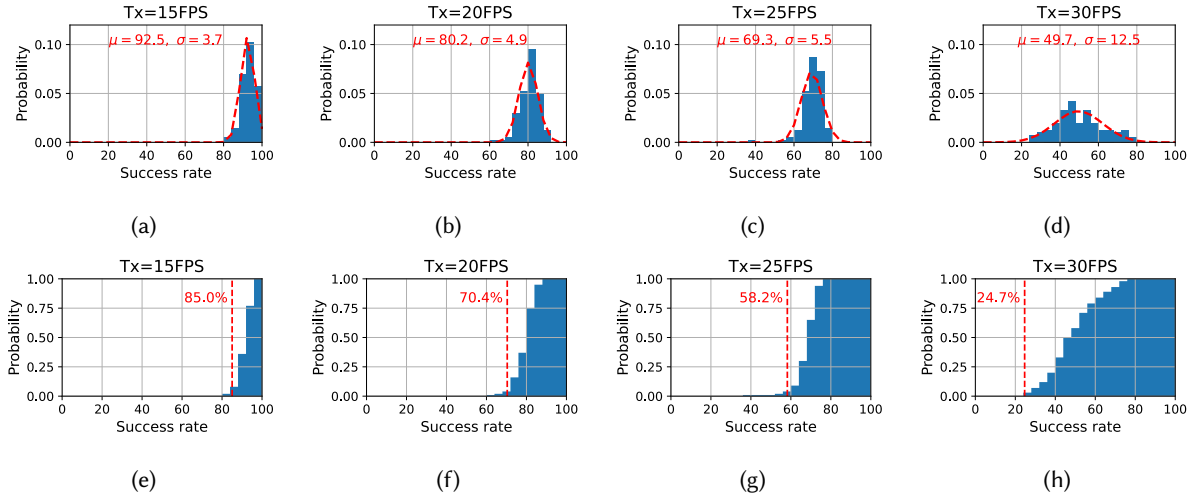[6]Source: https://github.com/Backblaze/JavaReedSolomon

Fig. 10. Figures (a) to (d): pdf of the success rate for 100 messages at different speeds (each message sends 100 QR codes). Figures (e) to (h): cdf with thresholds at $\mu - 2 \times \sigma$ to define the RS-FEC parameters.

A well-known FEC method is Reed-Solomon codes (RS-FEC), used also internally by QR codes to recover from errors. The basic principle is to add extra bytes (e) to the original data, so the link can recover from $\frac{e}{2}$ errors at any *unknown location* or from e erasures at *known locations*. SunBox implements RS-FEC using the first byte of each QR as a numbering sequence, thus the receiver knows the location of the missing QRs, and can recover from missing frames. We can assume that the decoded QRs are correct due to their internal RS-FEC and parity checks.

To provide an example of how to choose the parameters for RS-FEC, we use the statistical distribution of the success rate for an experiment considering 15 FPS at the transmitter and 30 FPS at the receiver. Figure 10a and Figure 10e depict the *pdf* and *cdf*, which follow a Gaussian distribution. Gaussians concentrate ~97% of their probability mass between $\mu \pm 2\sigma$. Hence, for this setup, designing a RS-FEC that can recover from 15 % of erasures ($\mu - 2\sigma = 85$ %) implies that 97% of the messages will be reliably delivered.

RS-FEC increases reliability but adds overhead. To distinguish the goodput of our system (in section 6), it is important to quantify the amount of overhead. Denoting N as the total number of QR codes in the message and B as the number of bytes in each QR code, the total amount of information is $N \times B$. But out of the N QR codes, only K carry data ($N - K$ carry redundancy), and each QR code has a sequence number to detect erasures (1 byte). Hence, the amount of application-level data is reduced to $K \times (B - 1)$, and the overhead ratio is given by:

$$O = \frac{(N - K) \times B + K}{N \times B} \tag{1}$$

In spite of this overhead, the strong advantage of RS is that the receiver only needs to get K out of N codes to successfully decode the message. It does not matter which K codes are received, it can be any combination. There are other erasure correction methods, such as rateless codes, which can adapt the data rate to the channel conditions. Those types of codes can be evaluated in future studies.

4.4 Reducing the Transmission Delay

Many screen-to-camera systems follow the Nyquist sampling theorem, where the camera's frame rate is set to twice the screen's [8, 11, 36]. This approach introduces an overhead since many frames are sampled twice. Due to

Table 3. Parameters for a system with $K = 54$ and a success rate of 97%

FPS	$\mu - 2\sigma$	N (frames)	Overhead	Duration (s)
15	85%	64	20.6 %	4.26
20	70%	77	34.0 %	3.85
25	58%	93	45.3 %	3.72
30	25%	216	89.1 %	7.20

(a) Transmitter components.   (b) Byte array to generate QR sequence.   (c) The SunBox prototype
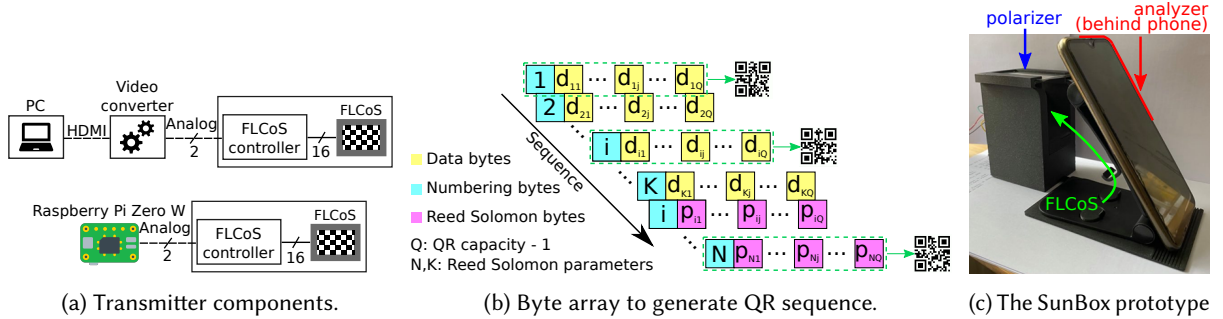
Fig. 11. The transmission system. In (b) yellow are the original data bytes, magenta the RS bytes and cyan the numbering bytes. Each row produces a QR.

this reason, some studies increase the frame rate at the transmitter. For example, Zhang et al. set the transmission rate to 29.9 FPS for a camera rate of 30 FPS [38], reducing in this manner the transmission delay to half compared to a camera transmitting at 15 FPS. We follow this latter approach to trade off a few packet losses for a reduction in delay. For SunBox, a few extra losses are not an issue because we have RS-FEC to overcome erasures.

To obtain the optimal transmission rate, we first estimate the number of error-correction packets ($N - K$) required for different screen rates, from 15 FPS to 30 FPS, in steps of 5 FPS. In all these experiments, the rate of the camera is kept at 30 FPS. The statistical distributions of these results are presented in Figure 10, where the threshold for a success rate of ∼97 % is set to $\mu - 2\sigma$ for all cases. Based on the determined thresholds ($\mu - 2\sigma$) and assuming $K = 54$ QR codes (application-level data), Table 3 estimates the total number of QR codes required by RS-FEC ($N = \frac{K}{\mu - 2\sigma}$, which includes data and redundancy); the overhead ratio (Equation 1); and the time required to receive the N frames at the given FPS (N/FPS). From that table, we can observe that, even though all the alternatives transmit K codes of data, the rates at 20 FPS and 25 FPS provide the shortest transmission delays. In section 6, we perform a more thorough evaluation and show that 20 FPS is the optimal transmission rate for various lighting conditions.

5 SYSTEM IMPLEMENTATION

On the basis of the previous experiments and observations, we now present a prototype for SunBox.

5.1 Transmitter

The main components of the transmitter are presented in Figure 11a. The steps to generate the video with the sequence of QR codes are as follows. First, a processor (in our case, a laptop or a Raspberry Pi Zero) generates the sequence of QR codes and adds the necessary numbering and error correction bytes. The complete information is arranged in a 2D array, as presented in Figure 11b. Each row includes a numbering byte and payload bytes. The
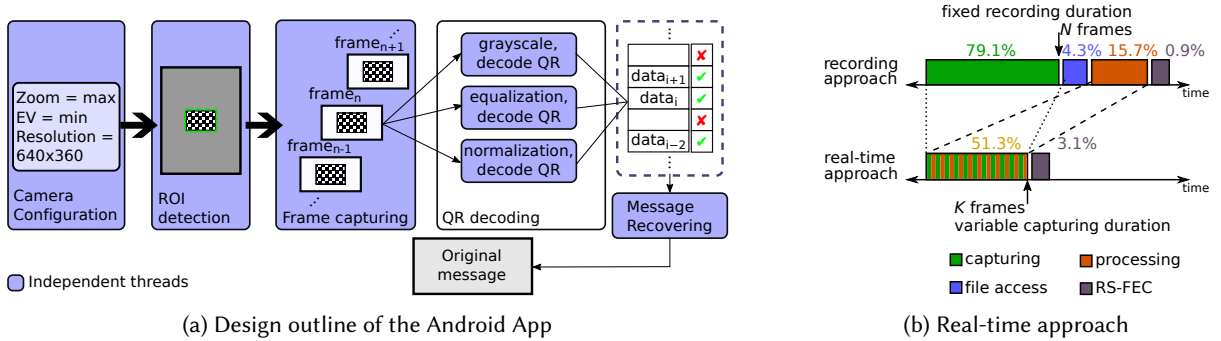
(a) Design outline of the Android App

(b) Real-time approach

Fig. 12. Description of the Android App. Note that for the recording approach in (b) the capture ends when N QR codes are received and for the real-time the capture stops earlier, when K QR codes are received.

payload represents either data or RS-FEC redundancy. This sequence is then converted to a video stream. Some processors (laptop) need a video converter, others (Raspberry Pi Zero) do not. The video converter adapts the signal to the format required by the FLCoS microdisplay. Finally, the FLCoS controller generates the signals to modulate each pixel of the matrix.

To assemble everything, we fabricate a small 3D-printed container and attach a phone holder, as shown in Figure 11c. The polarizer is placed on top of the container, and the FLCoS is inside the container. The encoded light is backscattered towards the smartphone. The analyzer is fixed within SunBox at an angle of 135° w.r.t the polarizer. The user's smartphone does not require any extra components for the system to work. The user simply has to push a button so the transmitter can start sending the video (continuously in a loop), and then, places the phone on top of the holder and starts the App to get the backscattered data.

5.2 Receiver

The receiver is a simple commercial smartphone. The main goals of our Android App design are to reduce the processing time and use of memory to allow SunBox to be used with any type of smartphone, including low-end devices. To accomplish these goals, our App performs four main tasks: camera configuration, ROI detection, frame capturing, QR decoding, and message recovering, as shown in Figure 12a.

Camera configuration. The first step is to configure the smartphone camera. By default, the App sets the zoom to its maximum value and the EV parameter to its lowest. The resolution is also a key parameter because it determines the quality of the image and the amount of memory used for processing. The App determines the best resolution automatically, based on the real-time capabilities of the phone, as described in the next section.

ROI detection. Following the method outlined in subsection 4.1, the program detects the FLCoS on the screen and, once detected, surrounds the FLCoS area with a rectangle in the UI and enables the capturing button.

Frame capturing. After the ROI is detected, the camera starts processing the frames in real-time. This step implements an extra optimization to reduce the delay. That optimization is explained next.

QR decoding. In this step, we enhance the image quality and decode the QR codes by applying the methods outlined in subsection 4.2. Three threads are run in parallel, each corresponding to an image processing method: *grayscale, equalization* and *normalization.* Each of these methods tries to decode a QR code. If any of the threads returns successfully, it kills the other threads, saves the data of the QR code into a queue, and marks the sequence number as 'present'. Otherwise, the QR code is marked as 'missing'.

Message recovery. In the last step, the *Reed Solomon* algorithm uses the QR-data queue and the 'present/missing' marks to recover the message. The *Backblaze* RS-FEC processing time depends on the capabilities of the phones

and the length of the message. In our experiments, we select the RS-FEC engine with N between 64 and 128, so low-end phones can run the algorithm.

The *frame capturing* process exploits the real-time features of Android using the *Camera2 API*. In general, a camera can capture a sequence of frames in real-time or record a video, Figure 12b compares both approaches. Given that most phones can operate in real-time at 30 FPS, we take the following steps:

- *Capturing.* Read a frame from the camera buffer instead of the internal storage (no *file access* stage).
- *Processing.* A frame's processing is done during the capturing of the next frame using multiple threads.
- *Decoding.* The final RS-FEC decoding process starts when K QRs are received, instead of waiting for all N.

To quantify the time saved, we implement both the recording and the real-time processing methods in Android. The run-time for the recording app is ~5.73 s and for the real-time app ~3.12 s. Figure 12b decomposes the amount of time taken by the individual steps of both approaches. A further improvement for the *capturing* stage would be to use the real-time feature at higher FPS (some phones are capable of operating at real-time with 60 FPS, c.f Table 5). However, we notice an image distortion when applying a zoom at that speed, rendering unreadable QR codes.

6 EVALUATION

In this section, we assess the SunBox system under different conditions using the setup presented in Figure 11c. Even though the FLCoS is inside a 3D case, any system using visible light modulation should check that there are no flickering effects. Given that the (backscattered) modulation is based on polarization, which is invisible to the human visual system, SunBox has no noticeable flickering effect. We asked five individuals to report if they noticed any flicker or disturbances while transmitting. All reported seeing a constant reflection from the FLCoS but without any flickering.

6.1 General Setup and Metrics

We assess SunBox under different conditions. Unless stated otherwise, the default settings are:

Message. The information sent by SunBox consists of a sequence of QR codes implementing RS(N,54): 54 QR codes for data and N total QR codes. After pushing a button in the transmitter, the video message is sent in a loop, thus the capture can start at any time.

Distance. The 3D casing provides a stable ~10 cm distance between the smartphone and the FLCoS transmitter. During capture, the phone is on the holder, not in the user's hands.

Camera. The phone is a Xiaomi Redmi 5A. The App sets automatically the resolution to 640×360, the zoom to the maximum value (8x), and the exposure value to the minimum (-2).

Light source. A desk lamp providing ~500 lx, which is the typical illumination in an office environment.

6.1.1 Goodput. Using the real-time approach, the app calculates the total time (t_{total}) from the start of the capture until the whole message is decoded. Denoting B as the number of bytes in a QR code, and recalling that $K = 54$, we define the goodput G based on an RS(N,K) as:

$$G = \frac{K \times (B - 1) \times 8}{t_{total}} \, [\, bps]$$ (2)

6.1.2 Message Success Rate. Because the QR sequence is displayed in a loop, if the receiver fails to receive enough QR codes in the first loop, it keeps capturing frames until it completes the necessary number of QR codes to run the RS-FEC algorithm. We consider a message to be successfully delivered if it is received within one iteration of the loop. Because the transmission rate (f_{Tx}) and the reception rate (f_{Rx}) do not match, the number of transmitted frames (N) is different from the number of received frames (N_{Rx}). The number of received frames is defined as:
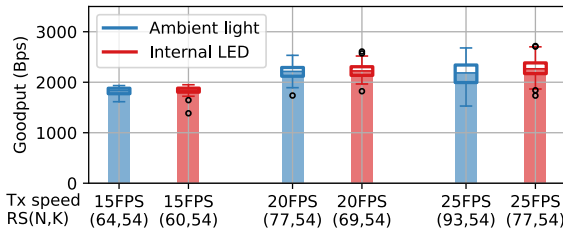
Fig. 13. Increasing the transmitter speed. The number of data QR codes $K = 54$ is the same for all transmission rates.
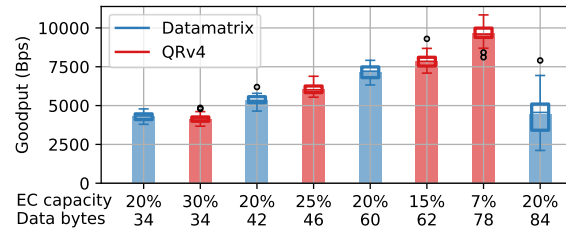
Fig. 14. Goodput performance for different error-correction rates for QR version 4 and different Datamatrices capacities.

$$N_{Rx} = N \times \frac{f_{Rx}}{f_{Tx}}. \tag{3}$$

The App has a progress bar that displays the number of unique frames received. We consider a message to be successfully delivered if the number of received frames is less than N_{Rx}.

6.2 Identifying the Optimal Transmission Rate

In subsection 4.4, we provide a preliminary analysis of the benefits of increasing the transmission speed beyond the Nyquist rule. Now, we test the system to identify the best transmission speed considering all the methods in section 4 and section 5. Figure 13 presents these results and shows that a transmission speed of 20 FPS, using an RS(77,54), has the highest goodput with low variance. Therefore, we set the system to use these parameters: $N = 77$, $K = 54$, and, we use Equation 3 to determine if a message is received successfully during the first loop (the number of received frames must be less than $N_{Rx} = 116$).

To showcase the strength of our approach, we compare the goodput of SunBox, which uses ambient light, against the goodput of the original FLCoS projector, which uses embedded LEDs. The results are presented in Figure 13. First, we determine the optimal RS parameters for the original system (because the use of the RGB LED requires less redundancy in the RS parameters). Then, we perform the experiments at different speeds. The results show no significant effect over the goodput, with the extra advantage that, removing the embedded LEDs reduces the power consumption (as described in subsection 6.9).

6.3 Analyzing the Effect of Zoom and Different Code Densities

After selecting the suitable speed, we evaluate the effect of the camera's zoom and the code density. The prior experiments use the maximum zoom provided by the Xiaomi phone (8x) and the lowest code density (QR v1). Our aim is to study the correlation between the applied zoom, the data density of the QR code, and the camera resolution. The evaluation considers three zoom levels (4x, 6x, and 8x) and four QR codes with capacities of 17, 32, 53, and 78 bytes, corresponding to versions 1, 2, 3, and 4, respectively. Additionally, if the success rate is lower than 90%, we increase the resolution of the camera from 640×360 to 960×720.

The results, in Figure 15, show two main results. First, even for the most basic phones in the market (30 FPS with 4x zoom, c.f. Table 5), SunBox provides a baseline performance above 2 kbps. Second, while basic phones (with a limited 4x zoom) would not benefit from increasing the code density and/or camera resolution, the majority of phones in the market would. Most medium-end phones provide an 8x zoom, which allows using dense codes (v4) to increase the goodput above 10 kbps, without the need to increase the camera resolution.
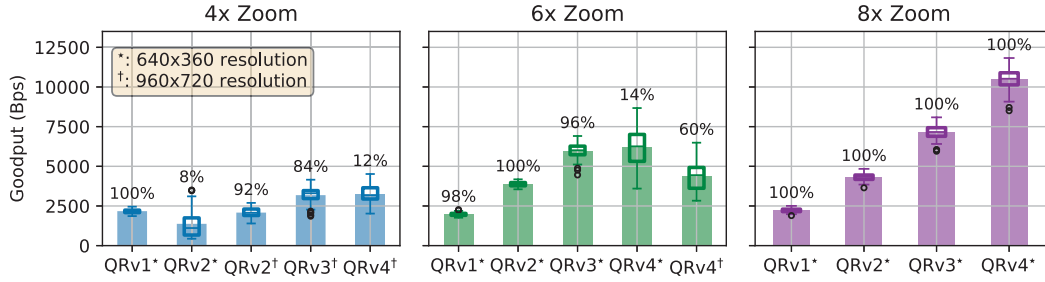
Fig. 15. Camera zoom effect on performance for different QR densities. For denser codes, we increase the resolution of the image. At the top of each bar is the message success rate.

6.4 Selecting the Best 2D Codes

As mentioned in subsection 2.5, two of the most widely used 2D codes are QR and Datamatrices. In this subsection, we identify the best code for SunBox. The main difference between QRs and Datamatrices is that QRs allow adjusting their error-correction rate, but Datamatrices do not. For example, QR version 4 provides four error-correction rates (7%, 15%, 25%, and 30%), while Datamatrices have a fixed rate of 20%. The higher the error-correction rate, the stronger the resilience of the message, but the lower the goodput.

Figure 14 compares QRs and Datamatrices containing a similar number of data bytes. Both codes provide a similar goodput when the error-correction rates of QRs are above 15%, but QRs significantly outperform Datamatrices with the lowest error-correction rate (7%). This occurs because, to maintain the 20% correction rate, the density required by Datamatrices is so high that the smartphone camera can no longer decode the messages reliably. Due to this insight, in the following sections, we keep the QR error-correction rate to the lowest value.

6.5 Analyzing the Effect of Light Intensity and Radiation Patterns

While artificial light is usually constant, we also evaluate the relationship between light intensity and SunBox's performance. Similar to subsection 6.3, our goal is to assess the resilience of the different code densities under various light conditions.

To control the light intensity, we add a dimmer to the setup. The results in Figure 17a show that SunBox is able to work even at very low light intensities. To put these results in context, it is important to note that 200 lx is the illumination required in a non-working environment (e.g. aisle), and 500 lx is the illumination required in a working setup (e.g. desk). QR version 4 starts failing only at 100 lx, versions 2 and 3 start failing with 50 lx, and version 1 continues to work even at 50 lx.

Intensity is not the only important parameter in lighting, the type of radiation (diffused or directed) is relevant as well. We find two main cases: rooms designed with (warm) *diffused* lights, such as living rooms; and rooms with (cold) *directed* lights, such as office spaces. SunBox operates without any modifications with warm diffuse lights, but with cold directed lights there are locations where the light is too intense. The issue and modification are depicted in Figure 16. Depending on the relative location between SunBox and the direct light source, in this case a ceiling light, the FLCoS may receive an intense beam that saturates the camera's sensor. To cope with this effect, a simple diffusing film can be placed over the polarizer, as shown in Figure 16a. This film distributes the focused light across the surface of the FLCoS, and its effect is demonstrated in Figure 16b and Figure 16c.

As shown in this section, SunBox is able to work with different types of *indoor ambient light*. However, as presented in subsection 6.8, we will see that natural sunlight presents other challenges.

(a) Setup using the ceiling lamp and the diffusing film.

(b) FLCoS reflection without the diffusing film.
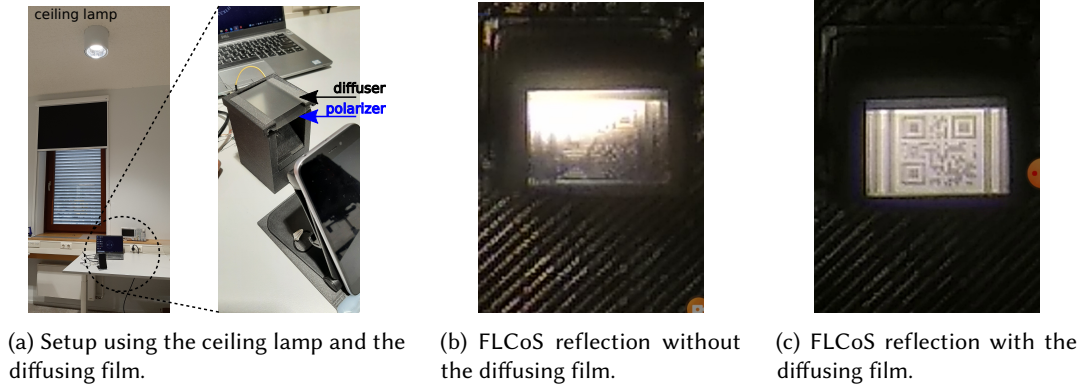
(c) FLCoS reflection with the diffusing film.

Fig. 16. Experiments in an office space (~500 lx) using a diffuser film for locations with strong light intensities. The image in (c) is clear enough to trigger the transmission.

6.6 Different Phone Orientations

In this section, we assess the performance of the system related to changes in the phone's position. We first change the phone's rotation, which makes the FLCoS appear inclined w.r.t. the camera. We use the QR version 4 and rotate the Xiaomi Redmi 5A phone 15° and 30°. The effect of the rotation, in Figure 17b and Figure 17c, is a larger ROI which causes a penalty in the goodput because the phone processes more pixels. Without rotation, SunBox provides more than 10 kbps, with a 15° rotation ~9.5 kbps, and with 30° ~9.0 kbps. These issues could be fixed with a more elaborated ROI detection method.

Another important requirement for the current version of SunBox is to use the phone holder. That is, the user has to place the phone on the 3D structure, instead of holding it with the hands. To show the importance of this requirement, we hold the phone in front of the analyzer, placing the wrists over the table where SunBox is located. We send information using QRs from version 1 to 4, and we notice that the success rate decreases for all densities, as presented in Table 4, being version 1 the most resilient to the user's handshaking. Overcoming this effect would require utilizing signal processing techniques that compensate for motion dynamics in smartphones [33].
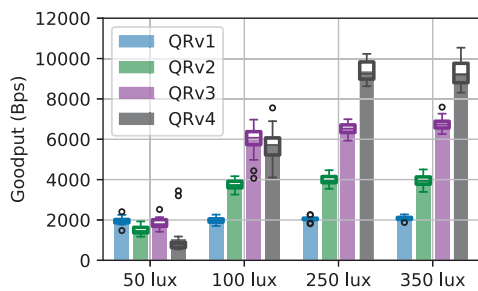
(a) Goodput for different artificial light intensities.
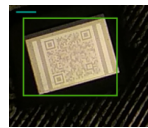
(b) ROI at 15°

(c) ROI at 30°

Table 4. Holding the phone by hand.

	Goodput	Success rate
QRv1	~2.0 kbps	90 %
QRv2	~3.6 kbps	75 %
QRv3	~4.9 kbps	50 %
QRv4	~5.3 kbps	10 %

Fig. 17. Results under different external conditions.

(a) Goodput of the system.
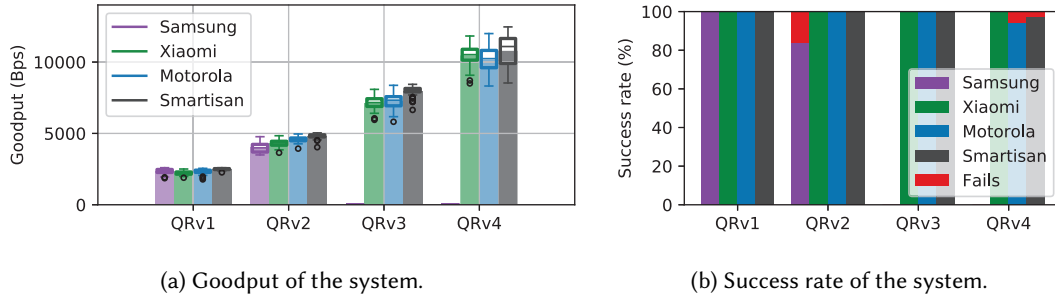
(b) Success rate of the system.

Fig. 18. Goodput and success rate for different QR versions and different smartphones with (artificial) ambient light.

6.7 Portability with Different Phone Models

Thus far, we have tested a single low-end phone (Xiaomi, 2017). To demonstrate the adaptability of SunBox, we test three other smartphones: a Samsung Galaxy A50, a Motorola Moto G6, and a Smartisan DE106. These phones are all low-end to mid-end phones launched a few years ago. Table 5 shows the features of each phone.

Table 5. Features of the phones used during the experiments.

Phone model	Year	Max. zoom	Resolution used	RAM	Size (mm)	Camera position	Camera Speed
Samsung Galaxy A50	2019	4x	1280×720	4 GB	158.5 x 74.7	Right	30 FPS
Xioami Redmi 5A	2017	8x	640×360	2 GB	140.4 x 70.1	Right	30 FPS
Morotorla Moto G6	2018	8x	640×360	3 GB	153.8 x 72.3	Center	30/60 FPS
Smartisan DE106	2018	8x	1280×764	8 GB	153.3 x 74.5	Right	30 FPS

The Samsung Galaxy A50 features a camera with a maximum zoom of 4x, thus, the App increases the resolution to 1280×720. The results in Figure 18 validate the relevance of the camera's zoom: even with the higher resolution, the Samsung phone is only able to work with the QRv1 and QRv2, the latter with a smaller success rate. With the denser versions QRv3 and QRv4, the Samsung phone is unable to receive any QR. The Motorola Moto G6 and the Xiaomi Redmi 5A have similar performance, working efficiently with all the QR code densities. For QRv4, the Motorola Moto G6 shows a slight increase in goodput variance and a slight decrease in the success rate. The Smartisan DE106 has more RAM, which allows faster image processing, providing a slightly higher goodput. However, the camera resolution has a big influence on the exposure value (EV), requiring a resolution of 1280×768 to work reliably. Overall, SunBox is able to operate reliably with different types of phones.

6.8 Natural Light

A critical difference between artificial and natural light is that the intensity and direction of natural light change over time. There is a significant difference between a clear day (tens of thousands of lux with light coming from mostly one direction) and a cloudy day (a few thousand lux with light coming from all directions). Furthermore, the geographical location (latitude) also impacts the amount of sunlight. We test SunBox during a challenging day in terms of sunlight: an overcast day during winter in the Northern Hemisphere, with some rain hours. We find that even on this challenging day, the system can successfully deliver messages from dawn to dusk. Similar to the experiments done in previous subsections, we test various code densities.

The setup of this experiment consists of placing the SunBox close to a large window and using the smartphone Xiaomi Redmi 5A as the receiver. The indoor light is turned off, so we are communicating only with sunlight.
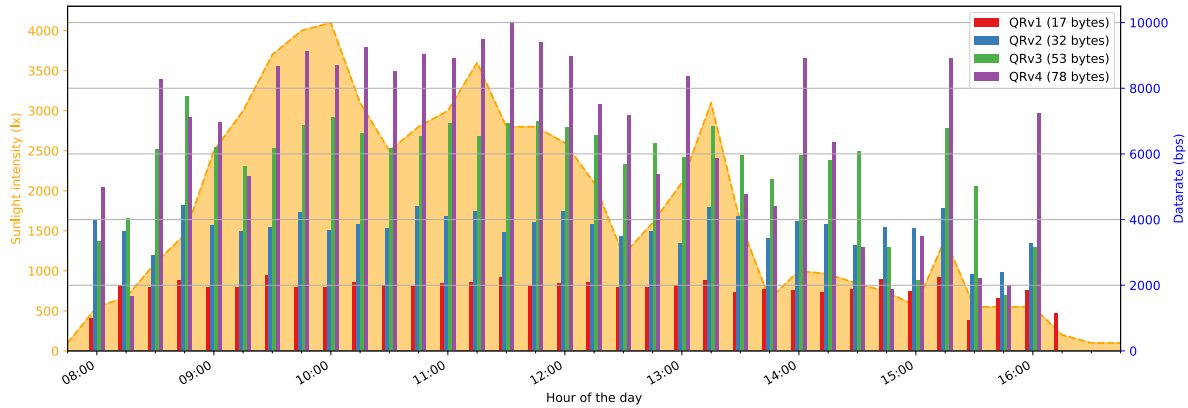
Fig. 19. SunBox performance using sunlight. Note: at 15:00, a light rain started.

Table 6. Message success rate with sunlight. The right column shows the period when the success rate was steady at 100%

QR Version	Bytes per QR	Message success rate	Range of 100% message success rate	Total Time
QRv1	17 bytes	100.0%	08:15 to 15:15	7h00m
QRv2	32 bytes	100.0%	08:15 to 15:15	7h00m
QRv3	53 bytes	89.7%	08:30 to 14:30	6h00m
QRv4	78 bytes	51.7%	09:30 to 12:00	2h30m

During an entire day, we send four messages every fifteen minutes, one corresponding to each QR version. Figure 19 and Table 6 show the results. The yellow background reflects the amount of sunlight (at 15:00, a light rain started), and the vertical bars capture the goodput with different data densities. We can observe that for sunlight intensities higher than 550 lx approximately, which occurs between 8:15 and 15:15 in a winter day (7h00m period), SunBox obtains an almost constant goodput for QRv1 and QRv2, 2 kbps, and 4 kbps respectively, with a 100% message success rate. For QRv3, the goodput is around 6 kbps but the 100% message success rate occurs between 8:30 and 14:30 (6h00m). This stable period starts with an intensity higher than 1100 lx but ends with an intensity of 800 lx. QRv4 has a 100% stable message success rate between 9:30 to 12:00 (3h00m) when the light intensity is over 2500 lx.

The key advantage of sunlight is that SunBox can be placed anywhere outdoors (we tested a few other outdoor locations with similar results), but we noticed an interesting phenomenon. At times, the goodput does not increase or decrease monotonically with the intensity of light. For example, during the period between 8:30 to 9:30, the sunlight intensity increases, but the goodput remains the same or even decreases. On the other hand, during the time 14:00 to 15:15, the goodput is high despite the low light intensity. Furthermore, SunBox only operates when the sunlight intensity is above a few hundred lux, while 50 lx were sufficient indoors. The reason for these phenomena is that, as stated before, not only the intensity of the ambient light matters but also its radiation pattern, which can change depending on the cloud conditions.

Overall, the results show that low-density codes, QRv1 and QRv2, are robust, attaining a 100% success rate for a long duration during a cloudy day (6h45m). The success rate of denser codes, on the other hand, tends to follow the intensity and radiation pattern of the ambient light. During summer or close to the equatorial line, SunBox would provide significantly better performance.

6.9 A Standalone System Running an Urban Application

Thus far, the experiments for SunBox have been performed using a laptop to provide the video input and power, and the payload has been text (a tale by Edgar Allan Poe, "The Black Cat"). In this section, we design a standalone system and develop a simple application based on Google Maps.

6.9.1 Standalone System. To demonstrate the potential of SunBox, we combine a few components to create a self-contained embedded system, as shown in Figure 20a:

- *Single board computer:* Raspberry Pi Zero W, which can produce the input signal required by the FLCoS without the need of a video converter. Cost: 10€, Power (consumption): 400 mW, low-power mode.
- *Battery and DC/DC booster:* A LP785060 lithium-ion polymer battery and an Adafruit Powerboost 1000C. In combination, they output 5 V to feed the board. Cost: 20€, Power (provided): up to 5 W.
- *Solar panel:* SLMD262K 10L from IXYS (220 mm x 126 mm x 2.1 mm) to charge the battery. Cost: 65€, Power (provided): up to 5 W, depending on illuminance.

Overall, the total cost is below 200€, and the solar cell provides enough power to run the system.

6.9.2 Power Analysis of Microdisplay. An important feature of using ambient light is the reduction in power consumption. To quantify the energy savings, we analyze the power consumption of the microdisplay.

The LCOS720 micro-projector has 4 different power supplies: VCC (supply for FLCoS panel), VIO (supply for I/O serial interface), DAVCC (supply for the embedded lights and their driver), and VCCX (supply for panel / EEPROM for LED calibration). In SunBox, we no longer need the DAVCC power supply, since the embedded lights are removed and the system communicates with ambient light. VCCX is used for color calibration of the embedded lights and is not needed either. We hypothesize VIO to be involved only in the start-up phase to configure the registers of the device, and it is not involved in the operation of the FLCoS. The nominal consumption of the entire micro-projector is 180 mW. However, considering only the VCC supply, which supports the operation of the FLCoS, the power consumption of the FLCoS core panel is 110 mW. Thus, if we could design a microdisplay for ambient light, the power consumption could be reduced by up to 40%.

(a) Standalone system, powered by a solar cell. (b) Selection screen. (c) ROI and data transmission. (d) Text output. (e) Map output.
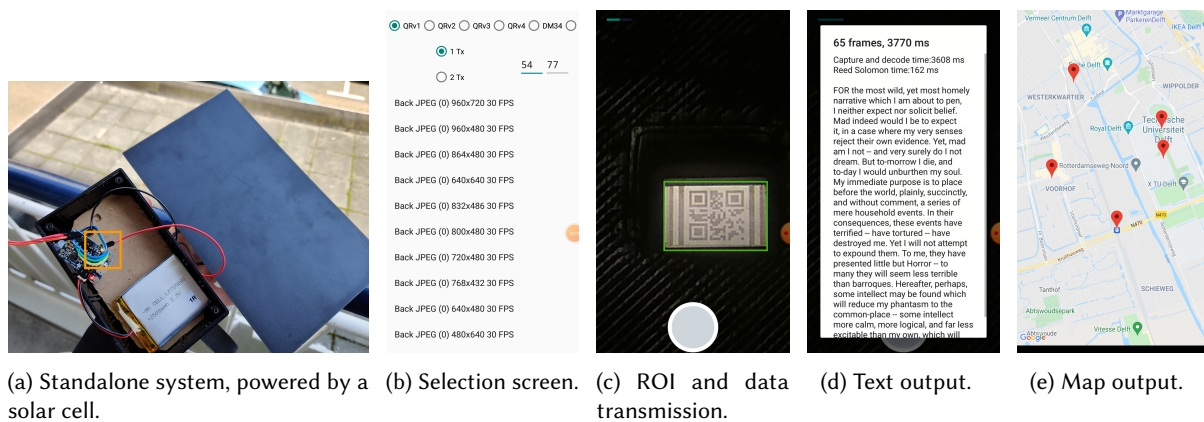
Fig. 20. SunBox standalone components (a) and App view. (b) Select different QR versions and camera resolutions. (c) The progress bar location is top-left. (d) Simple text output: fragment of *The black cat* by Edgar Allan Poe. (d) Markers on the map with transmitted coordinates.

6.9.3 An Urban Application. With SunBox as an embedded system, several transmitters could be deployed across a town for travelers to get coordinates for touristic places nearby. The user would not need to rely on any type of radio signal, she would only need to put the phone on the SunBox holder and get information for restaurants, events, museums, etc.

We develop a simple app based on Google Maps for this purpose, the screenshots of all the stages are presented in Figure 20:

1) We have a GUI to select the type of QR code, the values of N and K for RS-FEC, and to detect automatically all the possible configurations based on the real-time capabilities of the phone. This part does not need to be presented to the user. It is solely used to facilitate the evaluation of the different parameters.
2) The user starts the App, places the phone on the holder and the ROI is selected automatically. After the ROI is found, the user can push a button to start reading the video.
3) A green progress bar on the top left of the screen shows the number of received QR codes. When the App receives K unique QR codes, it stops and runs the RS-FEC algorithm to decode the message.
4) Initially we send only plain text. But sending geographical coordinates is simple too. The longitude and latitude contain 8-bytes each. Thus, even the least dense QR (version 1) can carry the coordinates for one location. The transmitter knows its location and sends coordinates for nearby places. The coordinates are then presented as markers in a map view using the GoogleMap SDK.

7 RELATED WORK

7.1 Liquid Crystal to Photo-diode

The first group of studies related to our work is systems that use LCs to modulate light and photo-diodes (PDs) at the receiver. For our purposes, we divide them into two groups: single-pixel and multi-pixel.

7.1.1 Single-pixel. These studies have a single LC surface at the transmitter and a single PD at the receiver. Due to the slow switching speed of the LC, their throughput is relatively low, around one kbps. Some of these studies require flashlights or lightbulbs to operate, such as *RetroVLC* [17] and *PassiveVLC* [32], while others can work with sunlight, like *LuxLink* [3] and *ChromaLux* [9].

7.1.2 Multi-pixel. To overcome the limited speed of single-pixel approaches, systems like *RetroTurbo* [31] and *RetroI2V* [29] use multiple LC surfaces at the transmitter and/or multiple PDs at the receiver, together with more sophisticated modulation schemes. These MIMO systems can reach speeds up to 8 kbps. However, they require transmitters with big surface areas and powerful artificial light sources that consume between 3 W and 30 W.

A common aspect of all the above systems (single- and multi-pixel) is that they use big *nematic* LCs, with surfaces of several tens of cm^2, and photodiodes, which are significantly faster receivers than cameras. SunBox uses a microdisplay with *smectic* LCs, which have different optical features. And, in spite of using low-end smartphones with slow cameras (30 FPS), we can exploit any type of ambient light (artificial or natural) to achieve speeds between 2 kbps to 10 kbps.

7.2 Camera as a Receiver

Other VLC systems exploit cameras as receivers instead of photodiodes. Cameras are slower but they have two appealing features: they are widely deployed in smartphones, and they have a 2D array of photo-sensors, which gives the advantage of spatial diversity. The key difference among these studies is the type of transmitter they use, and we identify three main groups.

7.2.1 LED to camera. These systems leverage the rolling shutter effect of cameras and require LEDs switching at kHz to transmit information. *Luxapose*[16] was one of the first methods to exploit this approach to transmit 8

Table 7. Different VLC systems

	Type	Source	Data rate	Power Tx	Range	Receiver	Outdoors
CVLC[18]	Active	3 RGB LED	>100 kbps	250 mW*	40 cm	Camera with lens	No‡
PassiveVLC[32]	Passive	LED Flashlight	1 kbps	400 μW + 3 W†	1 m	Photodiode	Yes
PIXEL[35]	Passive	Ambient Light	14 bps	1 mW	10 m	Camera	No‡
LuxLink[3]	Passive	Ambient light	80 bps	30 mW	(4.5–65) m	Photo-transistor	Yes
Chromalux[9]	Passive	Ambient light	1 kbps	27.3 mW	(1–50) m	Color sensor	Yes
RetroTurbo[31]	Passive	LED lamp	8 kbps	0.8 mW + 8 W†	7.5 m	Photodiode	No‡
SunBox	Passive	Ambient light	10 kbps	110 mW	10 cm	Camera	Yes

* Estimated value as no power consumption is reported. † Corresponds to the power of the LED used. ‡ No reported outdoor experiment.

symbols for indoor positioning. A more recent study proposes a more complex transmitter, using several LEDs to exploit the color and space dimensions, so the rolling shutter effect can still be exploited to achieve more than 100 kbps[18].

7.2.2   LED&LC to camera. Systems like POLI [4] combine RGB LEDs and LCs to transmit information exploiting the color dimension and achieving speeds ~500 bps. All the aforementioned systems (LED and LED&LC) need *active* control of the light source, which is something that SunBox does not require.

7.2.3   LC to camera. PIXEL [35] is the only study we found using ambient light and LCs to convey information, but the transmission is limited to 14 bps. Following a similar direction, systems such as *PolarTag* [26] do not modulate light *actively*, but they use a static 2D pattern, similar to a QR code, to change ambient light polarization and transmit static information. Like these LC-to-camera systems, we do not have active control over the light source, but by using a dynamic screen-like device, we can obtain speeds comparable to systems that modulate LEDs.

7.3   Screen to Camera

Several studies have leveraged screen-to-camera communication to achieve multi-pixel data transmission. Studies such as *ChromaCode* [37] and *Pixnet* [23] exploit standard displays to achieve data rates above 700 kbps and 12 Mbps, respectively, and their range can reach the order of meters. *COBRA* [11] and *RD Codes* [28] develop custom 2D color barcodes to attain data transmissions greater than 100 kbps at short ranges. *Softlight* [8] adds the concept of rateless codes for different channel conditions, *Uber-in-Light* [12] uses color channels and MFSK for high throughput and reliability, and *SBVLC*[36] implements a *"fast QR filtering"* for consecutive QR codes. All of these approaches make use of active screens on smartphones, except for *Uber-in-Light* which makes use of a traditional screen. Compared to our approach, we only use ambient light as the carrier of the system and use a microdisplay for secure short-range communication. Furthermore, our system works under sunlight, which reduces the performance of most screens or demands more power to increase the screen light intensity.

7.4   Reflective Displays

Overall, our work can be seen as an advancement at the intersection of the three areas mentioned above: *LCs* as transmitters, *cameras* as receivers, and *screens* as 2D surfaces with higher data densities. Our main motivation to merge these areas comes from reflective display technology [24], which exploits sunlight to backscatter images. Most of these reflective displays, however, are based on nematic LCs, making them slow, and are rather big. These two properties make them better suited for billboards. To create a secure and reliable link, we select a tiny microdisplay, which has the backscattering property but is not intended to work with ambient light due to

the use of smectic LCs. In principle, our approach could be extended to larger screens for long-range broadcast channel applications instead of short-range personal channels.

8 CONCLUSIONS

We propose a reliable short-range wireless system that exploits ambient light using a COTS microdisplay as a transmitter and a smartphone as the receiver. To the best of our knowledge, this work is the first to modulate ambient light using a screen-based on smectic LCs. SunBox obtains between 2 kbps and 10 kbps with a low-end phone (30 FPS) operating indoors, with standard lighting, and outdoors, during a cloudy day.

ACKNOWLEDGMENTS

REFERENCES

[1] Basler AG. 2021. Overlapping Image Acquisition. Retrieved November 12, 2021 from https://docs.baslerweb.com/overlapping-image-acquisition

[2] Karan Ahuja, Sujeath Pareddy, Robert Xiao, Mayank Goel, and Chris Harrison. 2019. LightAnchors: Appropriating Point Lights for Spatially-Anchored Augmented Reality Interfaces. In *Proceedings of the 32nd Annual ACM Symposium on User Interface Software and Technology* (New Orleans, LA, USA) *(UIST '19)*. ACM, New York, NY, USA, 189–196. https://doi.org/10.1145/3332165.3347884

[3] Rens Bloom, Marco Zúñiga Zamalloa, and Chaitra Pai. 2019. LuxLink: Creating a Wireless Link from Ambient Light. In *Proceedings of the 17th Conference on Embedded Networked Sensor Systems* (New York, New York, USA) *(SenSys '19)*. ACM, New York, NY, USA, 166–178. https://doi.org/10.1145/3356250.3360021

[4] Chun-Ling Chan, Hsin-Mu Tsai, and Kate Ching-Ju Lin. 2017. POLI: Long-Range Visible Light Communications Using Polarized Light Intensity Modulation. In *Proceedings of the 15th Annual International Conference on Mobile Systems, Applications, and Services* (Niagara Falls, New York, USA) *(MobiSys '17)*. ACM, New York, NY, USA, 109–120. https://doi.org/10.1145/3081333.3081353

[5] Ryan Chylinski. 2012. *Time-lapse photography: A Complete Introduction to Shooting, Processing, and Rendering Time-lapse Movies with a DSLR Camera*. Cedar Wings Creative.

[6] Trong-Hop Do and Myungsik Yoo. 2017. Two-Dimensional Coding for Optical Camera Communication using CMOS Sensors. In *International Conference on Information and Communications 2017* (Hanoi, Vietnam) *(ICIC '17)*. IEEE, New York, NY, USA, 314. https://doi.org/10.1109/ICIC42290.2017

[7] David Doroski, Stephen H Perlmutter, and Garret Moddel. 1994. Alignment layers for improved surface-stabilized ferroelectric liquid-crystal devices. *Appl. Opt.* 33, 13 (1994), 2608–2610. https://doi.org/10.1364/AO.33.002608

[8] Wan Du, Jansen Christian Liando, and Mo Li. 2016. Softlight: Adaptive visible light communication over screen-camera links. In *IEEE INFOCOM 2016-The 35th Annual IEEE International Conference on Computer Communications* (San Francisco, CA, USA) *(INFOCOM '16)*. IEEE, New York, NY, USA, 1–9. https://doi.org/10.1109/INFOCOM.2016.7524510

[9] Seyed Keyarash Ghiasi, Marco A. Zúñiga Zamalloa, and Koen Langendoen. 2021. A Principled Design for Passive Light Communication. In *Proceedings of the 27th Annual International Conference on Mobile Computing and Networking* (New Orleans, Louisiana) *(MobiCom '21)*. ACM, New York, NY, USA, 121–133. https://doi.org/10.1145/3447993.3448629

[10] Qi Guo, Kexin Yan, Vladimir Chigrinov, Huijie Zhao, and Michael Tribelsky. 2019. Ferroelectric Liquid Crystals: Physics and Applications. *Crystals* 9, 9, Article 470 (2019), 21 pages. https://doi.org/10.3390/cryst9090470

[11] Tian Hao, Ruogu Zhou, and Guoliang Xing. 2012. COBRA: Color Barcode Streaming for Smartphone Systems. In *Proceedings of the 10th International Conference on Mobile Systems, Applications, and Services* (Low Wood Bay, Lake District, UK) *(MobiSys '12)*. ACM, New York, NY, USA, 85–98. https://doi.org/10.1145/2307636.2307645

[12] Mostafa Izz, Zhongyuan Li, Hongbo Liu, Yingying Chen, and Feng Li. 2016. Uber-in-light: Unobtrusive visible light communication leveraging complementary color channel. In *IEEE INFOCOM 2016-The 35th Annual IEEE International Conference on Computer Communications* (San Francisco, CA, USA) *(INFOCOM '16)*. IEEE, New York, NY, USA, 1–9. https://doi.org/10.1109/INFOCOM.2016.7524513

[13] Weiwei Jiang, Denzil Ferreira, Jani Ylioja, Jorge Goncalves, and Vassilis Kostakos. 2014. Pulse: Low Bitrate Wireless Magnetic Communication for Smartphones. In *Proceedings of the 2014 ACM International Joint Conference on Pervasive and Ubiquitous Computing* (Seattle, Washington) *(UbiComp '14)*. ACM, New York, NY, USA, 261–265. https://doi.org/10.1145/2632048.2632094

[14] J.C. Jones, M.J. Towler, and J.R. Hughes. 1993. Fast, high-contrast ferroelectric liquid crystal displays and the role of dielectric biaxiality. *Displays* 14, 2 (April 1993), 86–93. https://doi.org/10.1016/0141-9382(93)90075-G

[15] Sung-Yoon Jung, Ji-Hwan Lee, Wonwoo Nam, and Byung Wook Kim. 2020. Complementary Color Barcode-Based Optical Camera Communications. *Wireless Communications and Mobile Computing* 2020, 1, Article 3898427 (Feb. 2020), 8 pages. https://doi.org/10.1155/2020/3898427

[16] Ye-Sheng Kuo, Pat Pannuto, Ko-Jen Hsiao, and Prabal Dutta. 2014. Luxapose: Indoor Positioning with Mobile Phones and Visible Light. In *Proceedings of the 20th Annual International Conference on Mobile Computing and Networking* (Maui, Hawaii, USA) *(MobiCom '14)*. ACM, New York, NY, USA, 447–458. https://doi.org/10.1145/2639108.2639109

[17] Jiangtao Li, Angli Liu, Guobin Shen, Liqun Li, Chao Sun, and Feng Zhao. 2015. *Retro-VLC*: Enabling Battery-Free Duplex Visible Light Communication for Mobile and IoT Applications. In *Proceedings of the 16th International Workshop on Mobile Computing Systems and Applications* (Santa Fe, New Mexico, USA) *(HotMobile '15)*. ACM, New York, NY, USA, 21–26. https://doi.org/10.1145/2699343.2699354

[18] Liqiong Liu, Rui Deng, Jin Shi, Jing He, and Lian-Kuan Chen. 2020. Beyond 100-kbit/s Transmission over Rolling Shutter Camera-based VLC Enabled by Color and Spatial Multiplexing. In *Proceedings of the Optical Fiber Communication Conference (OFC) 2020* (San Diego, California, USA) *(OFC '20)*. Optica Publishing Group, Washington DC, USA, M1J.4. https://doi.org/10.1364/OFC.2020.M1J.4

[19] Wenkai Liu, Biqi Wang, Yan Li, and Menglong Wu. 2020. Screen-Camera Communication System Based on Dynamic QR Code. *IOP Conference Series: Materials Science and Engineering* 790, 1, Article 012012 (March 2020), 6 pages. https://doi.org/10.1088/1757-899X/790/1/012012

[20] Control Electronic Co. Ltd. 2020. 0.2 inch FLCOS Micro Display Module for 720x540 HMD, Video Glasses. Retrieved November 12, 2021 from http://www.szcontrol.com/Index/pdetail/id/305.html

[21] Antonio Martínez-García, Ignacio Moreno, María M. Sánchez-López, and Pascuala García-Martínez. 2009. Operational modes of a ferroelectric LCoS modulator for displaying binary polarization, amplitude, and phase diffraction gratings. *Appl. Opt.* 48, 15 (May 2009), 2903–2914. https://doi.org/10.1364/AO.48.002903

[22] Hao Pan, Yi-Chao Chen, Guangtao Xue, and Xiaoyu Ji. 2017. MagneComm: Magnetometer-Based Near-Field Communication. In *Proceedings of the 23rd Annual International Conference on Mobile Computing and Networking* (Snowbird, Utah, USA) *(MobiCom '17)*. ACM, New York, NY, USA, 167–179. https://doi.org/10.1145/3117811.3117824

[23] Samuel David Perli, Nabeel Ahmed, and Dina Katabi. 2010. PixNet: Interference-Free Wireless Links Using LCD-Camera Pairs. In *Proceedings of the Sixteenth Annual International Conference on Mobile Computing and Networking* (Chicago, Illinois, USA) *(MobiCom '10)*. ACM, New York, NY, USA, 137–148. https://doi.org/10.1145/1859995.1860012

[24] Samsung. 2017. Reflective Display Technology. Retrieved November 12, 2021 from https://pid.samsungdisplay.com/en/learning-center/blog/reflective-display-technology

[25] Shuyu Shi, Lin Chen, Wenjun Hu, and Marco Gruteser. 2015. Reading between Lines: High-Rate, Non-Intrusive Visual Codes within Regular Videos via ImplicitCode. In *Proceedings of the 2015 ACM International Joint Conference on Pervasive and Ubiquitous Computing* (Osaka, Japan) *(UbiComp '15)*. ACM, New York, NY, USA, 157–168. https://doi.org/10.1145/2750858.2805824

[26] Zhao Tian, Charles J. Carver, Qijia Shao, Monika Roznere, Alberto Quattrini Li, and Xia Zhou. 2020. PolarTag: Invisible Data with Light Polarization. In *Proceedings of the 21st International Workshop on Mobile Computing Systems and Applications* (Austin, TX, USA) *(HotMobile '20)*. ACM, New York, NY, USA, 74–79. https://doi.org/10.1145/3376897.3377854

[27] Anran Wang, Zhuoran Li, Chunyi Peng, Guobin Shen, Gan Fang, and Bing Zeng. 2015. InFrame++: Achieve Simultaneous Screen-Human Viewing and Hidden Screen-Camera Communication. In *Proceedings of the 13th Annual International Conference on Mobile Systems, Applications, and Services* (Florence, Italy) *(MobiSys '15)*. ACM, New York, NY, USA, 181–195. https://doi.org/10.1145/2742647.2742652

[28] Anran Wang, Shuai Ma, Chunming Hu, Jinpeng Huai, Chunyi Peng, and Guobin Shen. 2014. Enhancing Reliability to Boost the Throughput over Screen-Camera Links. In *Proceedings of the 20th Annual International Conference on Mobile Computing and Networking* (Maui, Hawaii, USA) *(MobiCom '14)*. ACM, New York, NY, USA, 41–52. https://doi.org/10.1145/2639108.2639135

[29] Purui Wang, Lilei Feng, Guojun Chen, Chenren Xu, Yue Wu, Kenuo Xu, Guobin Shen, Kuntai Du, Gang Huang, and Xuanzhe Liu. 2020. Renovating Road Signs for Infrastructure-to-Vehicle Networking: A Visible Light Backscatter Communication and Networking Approach. In *Proceedings of the 26th Annual International Conference on Mobile Computing and Networking* (London, United Kingdom) *(MobiCom '20)*. ACM, New York, NY, USA, Article 6, 13 pages. https://doi.org/10.1145/3372224.3380883

[30] Maury Wright. 2015. Philips Lighting deploys LED-based indoor positioning in Carrefour hypermarket. Retrieved November 12, 2021 from https://goo.gl/a0tGIj

[31] Yue Wu, Purui Wang, Kenuo Xu, Lilei Feng, and Chenren Xu. 2020. Turboboosting Visible Light Backscatter Communication. In *Proceedings of the Annual Conference of the ACM Special Interest Group on Data Communication on the Applications, Technologies, Architectures, and Protocols for Computer Communication* (Virtual Event, USA) *(SIGCOMM '20)*. ACM, New York, NY, USA, 186–197. https://doi.org/10.1145/3387514.3406229

[32] Xieyang Xu, Yang Shen, Junrui Yang, Chenren Xu, Guobin Shen, Guojun Chen, and Yunzhe Ni. 2017. PassiveVLC: Enabling Practical Visible Light Backscatter Communication for Battery-Free IoT Applications. In *Proceedings of the 23rd Annual International Conference on Mobile Computing and Networking* (Snowbird, Utah, USA) *(MobiCom '17)*. ACM, New York, NY, USA, 180–192. https://doi.org/10.

1145/3117811.3117843

[33] Jackie (Junrui) Yang and James A. Landay. 2019. InfoLED: Augmenting LED Indicator Lights for Device Positioning and Communication. In *Proceedings of the 32nd Annual ACM Symposium on User Interface Software and Technology* (New Orleans, LA, USA) *(UIST '19)*. ACM, New York, NY, USA, 175–187. https://doi.org/10.1145/3332165.3347954

[34] Yanbing Yang, Jun Luo, Chen Chen, Zequn Chen, Wen-De Zhong, and Liangyin Chen. 2021. Pushing the Data Rate of Practical VLC via Combinatorial Light Emission. *IEEE Transactions on Mobile Computing* 20, 5 (May 2021), 1979–1992. https://doi.org/10.1109/TMC.2020.2971204

[35] Zhice Yang, Zeyu Wang, Jiansong Zhang, Chenyu Huang, and Qian Zhang. 2015. Wearables Can Afford: Light-Weight Indoor Positioning with Visible Light. In *Proceedings of the 13th Annual International Conference on Mobile Systems, Applications, and Services* (Florence, Italy) *(MobiSys '15)*. ACM, New York, NY, USA, 317–330. https://doi.org/10.1145/2742647.2742648

[36] Bingsheng Zhang, Kui Ren, Guoliang Xing, Xinwen Fu, and Cong Wang. 2015. SBVLC: Secure barcode-based visible light communication for smartphones. *IEEE Transactions on Mobile Computing* 15, 2 (Feb. 2015), 432–446. https://doi.org/10.1109/TMC.2015.2413791

[37] Kai Zhang, Yi Zhao, Chenshu Wu, Chaofan Yang, Kehong Huang, Chunyi Peng, Yunhao Liu, and Zheng Yang. 2021. ChromaCode: A Fully Imperceptible Screen-Camera Communication System. *IEEE Transactions on Mobile Computing* 20, 3 (March 2021), 861–876. https://doi.org/10.1109/TMC.2019.2956493

[38] Ouyang Zhang, Zhenzhi Qian, Yifan Mao, Kannan Srinivasan, and Ness B. Shroff. 2019. ERSCC: Enable Efficient and Reliable Screen-Camera Communication. In *Proceedings of the Twentieth ACM International Symposium on Mobile Ad Hoc Networking and Computing* (Catania, Italy) *(Mobihoc '19)*. ACM, New York, NY, USA, 281–290. https://doi.org/10.1145/3323679.3326526